The `multitaper` spectrum analysis package in Python

Germán A. Prieto[1]
[1] Departamento de Geociencias, Universidad Nacional de Colombia
[*] Corresponding author: Germán A. Prieto (gaprietogo@unal.edu.co)

Preprint of accepted paper in Seismological Research Letters (2022).

ABSTRACT

Spectral analysis has been a fundamental tool in analyzing seismic signals for studying the earthquake source, propagation of seismic waveforms through the Earth and even monitoring changes in Earth's structure. I present an open-source Python package, **`multitaper`**, for spectral analysis using the multitaper algorithm. The package not only includes power spectral density (PSD) estimation (with confidence intervals), but also bivariate problems including coherence, dual-frequency correlations, and deconvolution estimation. Implementation of the sine and quadratic multitaper algorithms are also available. For the reader to quickly learn how to use the package I briefly present several examples using earthquake records from the 2019 M6.0 Mesetas, Colombia earthquake and its aftershocks recorded at regional distances for estimating time-frequency spectrograms, spectral ratio and source time functions, and correlations between neighboring frequencies. Jupyter Notebooks are shared to reproduce the figures.

Keywords: multitaper, python, spectral analysis, deconvolution .

Introduction

Spectral analysis if a fundamental tool for the analysis of time and spatial series in geophysics (Bath, 2012; Tary et al., 2019, Dannemann et al., 2021). The objective of spectral analysis is the characterization of a time (or space) series, that is, to quantitatively say (1) what its frequency content is, (2) how one series differs from another or (3) how two series are related. These three aspects are described in the frequency domain using the power spectral density (PSD), the spectral coherency and the transfer (or frequency response) functions respectively, or their time domain counterparts the autocovariance, the cross-correlation and the impulse response (Bracewell, 1986; Percival and Walden, 1993).

Recent seismological applications of spectral analysis and the use of the functions listed above are broad, including earthquake source estimation (Madariaga et al., 2019; Chaves et al., 2020; Trugman and Savvaidis, 2021), attenuation tomography (Jang et al., 2019), crust and mantle structure (Cossette et al., 2016; Liu et al., 2018), characterizing GNSS sensors and ambient noise (Qin et al., 2019; Melgar et al., 2020a, 2020b), array and Large-N seismology (Gibbons et al., 2017; Kemna et al., 2020), seismic interferometry and structural health monitoring (Kong et al., 2018; Bonilla et al., 2019; Morelli et al., 2021; Häusler et al., 2021) and much more.

Methods for estimation of the spectrum include parametric and non-parametric methods. The first method (Olafsson, 1995; Diagourtas et al., 2001; Ugalde et al., 2021) is generally approached using autoregressive models (AR, ARMA, ARIMA, etc.), but is not the focus of this contribution.

The second method (the focus of this contribution) usually employs the fast Fourier transform (FFT) of a discretely sampled data set after applying a taper (windowing). This approach is computationally efficient but comes with its limitations; the frequency resolution is bounded by the data length, and it suffers from spectral leakage – the tendency for energy from distant frequencies to appear in the frequency of interest (Kay and Marple, 1981, Prieto et al., 2007). In addition, the variance of the spectrum estimate is large and in many cases averaging of nearby frequencies are required.

The multitaper algorithm first proposed by Thomson (1982) addresses this trade-off between bias and variance. It aims at reducing the bias by tapering using the orthogonal Slepian sequences that are constructed to optimally reduce spectral leakage and, as its name suggests, multiple independent estimates of the spectrum are averaged to reduce variance.

There are already several freely available codes that implement the multitaper algorithm in Fortran 77 (Pardo-Igúzquiza et al., 1994), Julia (Haley & Geoga, 2020), R (Rahim et al., 2014), C (Lees and Park, 1995), and Fortran 90 (Prieto et al., 2009). Python implementations or wrapper of some of these codes include pymutt (code.google.com/archive/p/pymutt/) and mtspec (krischer.github.io/mtspec/), the latter providing most features to the ones available here. The `multitaper` package (this contribution) is a translation of the Fortran90 (Prieto et al., 2009) codes in Python and provides a unified platform for spectral analysis. It creates a Python class (*MTSpec*) with the resulting multitaper estimate of the PSD, but can provide further information including confidence intervals, line detection, quadratic inverse PSD, etc. In the case of studying two time series another Python class (MTCross) is used. Unique features in this package include

bi-variate dual-frequency coherence and cross-correlations. In the following I will provide 3 seismological examples on the use of **`multitaper`**. Jupyter Notebooks to reproduce the figures in this paper and those of Prieto et al. (2009) are made available.

Multitaper spectrum analysis

The multitaper algorithm is like other non-parametric spectral estimates in that the *N*-long time sequence y_n studied ($n=0,1,...N$) is multiplied by the kth taper v_k and then Fourier transformed

$$Y_k = \sum_{n=0}^{N-1} y_n \, v_k e^{-2\pi i f n} \,, \quad (1)$$

but instead of using a single taper a K number of orthogonal tapers are applied such that the power spectral density (PSD) estimate $\hat{S}$ is:

$$\hat{S}_y(f) = \frac{\sum_{k=0}^{K-1} w_k |Y_k(f)|}{\sum_{k=0}^{K-1} w_k}, \quad (2)$$

a weighted average of the Y_k's, where the w_k are weights designed to reduce spectral leakage while keeping the variance of the estimate low (see Thomson, 1982; Prieto et al, 2009). The choice of weights w_k can be selected based on the eigenvalues of the tapers or using an adaptive weighting (Thomson, 1982). The quadratic multitaper estimate (Prieto et al., 2007) uses the second derivative of the spectrum to obtain a higher resolution estimate of the spectrum.

When working with two time series x and y, and for simplicity assuming $w_k=1$ the estimate of the cross-spectrum is:

$$\hat{S}_{xy}(f) = \sum_{k=0}^{K} X_k(f) Y_k^*(f), \quad (3)$$

and the coherency and transfer functions are:

$$\hat{C}_{xy}(f) = \frac{S_{xy}(f)}{\sqrt{S_x(f)}\sqrt{S_y(f)}}, \quad (4)$$

$$\hat{T}_{xy}(f) = \frac{S_{xy}(f)}{S_Y(f)} \,, \quad (5)$$

The squared of C_{xy} is called the squared coherence and has values between 0 and 1 and represents the similarity of the two waveforms (it is analogous to the cross-correlation). **`multitaper`** allows to take the inverse Fourier transform on these three estimates to obtain the cross-correlation, normalized cross-correlation and the deconvolution between the two signals.

For non-stationary signals the spectra at distant frequencies are correlated (Thomson and Vernon, 1998; Larsen and Hanssen 2004; Prieto et al., 2005) the dual-frequency coherency (DFC) – a matrix of spectral coherence between frequencies (f_1,f_2) – can be estimated as:

$$\hat{C}_{xy}(f_1, f_2) = \frac{\sum_{k=0}^{K} X_k(f_1) Y_k^*(f_2)}{\sqrt{S_x(f_1)}\sqrt{S_y(f_2)}}, \quad (6)$$

If the DFC is estimated for a single time series, the main diagonal of the matrix (f_1=f_2) has unit amplitude, while the off-diagonal term's amplitudes will depend on the nature of the signal (diffusive, non-stationarity, etc.). If the DFC is estimated for two distinct time series, the main diagonal represents the coherence (as in equation 4). The off-diagonal terms reflect the correlation between the spectra at distant frequencies, for example for dispersive or diffusive signals (see examples in Mellors et al., 1998; Prieto et al., 2005; Liu and Ben Zion, 2016, 2018; Liu and Beroza, 2020).

Data

In this work 3 examples using seismological data are presented. All examples use records of the M6.0 Mesetas earthquake and its aftershocks (Mayorga et al., 2020; Noriega-Londoño, 2021) on December 24th, 2019, recorded at regional distances by stations from the Servicio Geológico Colombiano (SGC) and a temporary deployment inside a 14-story building in downtown Bogota (Jaimes et al., 2022). The 2019 M6.0 Mesetas earthquake was followed by a M5.8 aftershock just 15 minutes later (see Figure 1). In the following months at least 20 M4+ earthquakes were located in the mainshock area (see Data and Resources).

Time varying response of a building

Figure 1 shows the recorded ground motions of the horizontal component at the 14th floor of the Crisanto building in downtown Bogota (Jaimes et al., 2022). Both the M6.0 and M5.8 earthquakes are clearly visible and some M4+ in between are also evident. The time-frequency spectrogram shown is calculated for 20-second-long windows with a 50% overlap using the adaptive and quadratic multitaper estimates (see pseudo-code 1):

Pseudo-Code 1 - Spectrogram

```
import multitaper.mtspec as spec
t,freq,qi,adap = spec.spectrogram(x,dt,twin=20.,olap=0.5,
                                  nw,kspec)
```

where *x* is the entire trace shown in Figure 1 *nw*, *kspec*, and *dt* are the time-bandwidth product, the number of tapers to use and the sampling rate respectively and `twin` and `olap` tell the function the length of each window and the proportion of overlap for constructing the spectrogram. The function returns the time and frequency vectors *t, freq* and the quadratic and adaptive spectrum estimates *qi, adap*.

For each 20-second window the function calls the multitaper modules (Pseudo-code 2):

Pseudo-Code 2 - Individual spectra

```
from multitaper import MTSpec
psd    = MTSpec(y,nw,kspec,dt)
freq   = psd.freq
adap0   = psd.spec
qi0 = psd.qiinv()[0]
```

where *y* is the 20 second waveform (cut from the entire trace), The adaptive spectrum *adap0* as well as the quadratic estimate *qi0* for a single window can be requested from the *psd* variable.

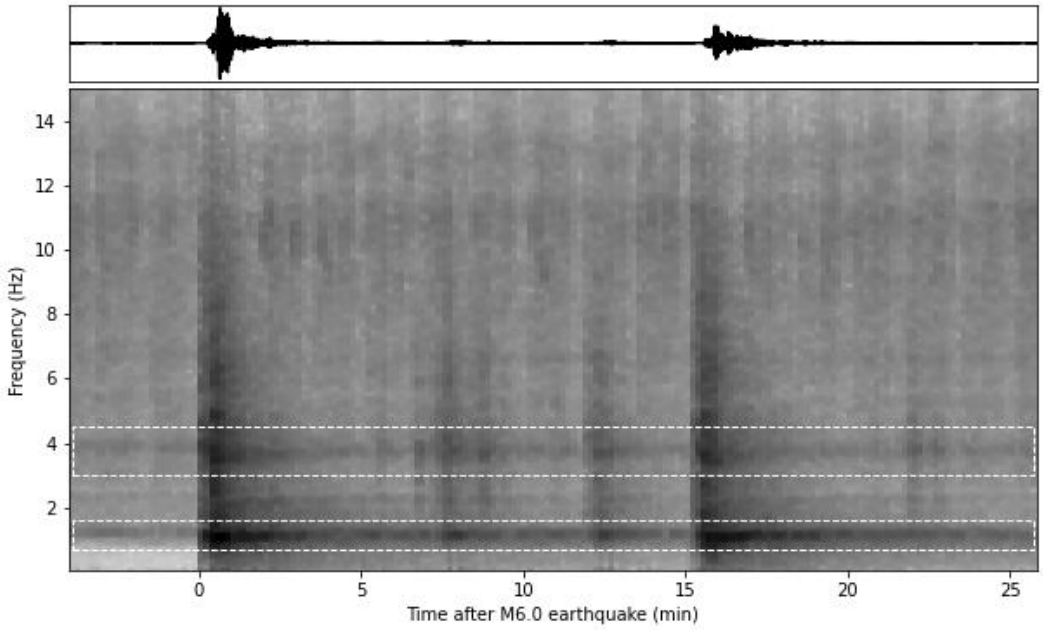

Figure 1: Time-frequency spectrogram of the M6.0 Mesetas earthquake recorded at a station on the 14th floor in downtown Bogota (150 km north). The recorded acceleration records (top panel) and corresponding spectrogram (bottom panel, using the quadratic multitaper) show the clear presence of at least 4 aftershocks including a M5.8 15 minutes later. White boxes highlight the vibrational modes of the building (see Figure 2).

Figure 2 shows a comparison of the adaptive multitaper estimate (*adap*) and the quadratic multitaper (`qi`) spectrograms around two of the natural frequencies of the building at about 1.25 Hz and 3.9 Hz. In both cases a dramatic decrease of the natural frequencies is observed after the two largest earthquakes and the frequencies have not fully recovered after 25 minutes. The quadratic estimate has higher resolution (better resolved peak) than the adaptive multitaper and is best for tracking the frequency wander of the natural frequencies (Clinton et al., 2006).

Earthquake source time functions and spectral ratio

Figure 3 shows the seismic records of the M6.0 and M5.8 earthquakes recorded at station PRA about 140 km from the earthquake epicenter. Two M4+ earthquakes are also shown that will be used as empirical Green's functions (EGF) to remove the effects of propagation, attenuation, and site from the estimated spectrum (Mueller, 1985; Hough, 1997; Abercrombie, 2005). The amplitude spectra of the mainshock and its EGF are also shown along with the amplitude spectrum of a noise window (for assessing the signal-to-noise ratio). A similar code as in Pseudo-Code 2 is used for estimating the amplitude spectrum, except for normalizing and taking the square root.

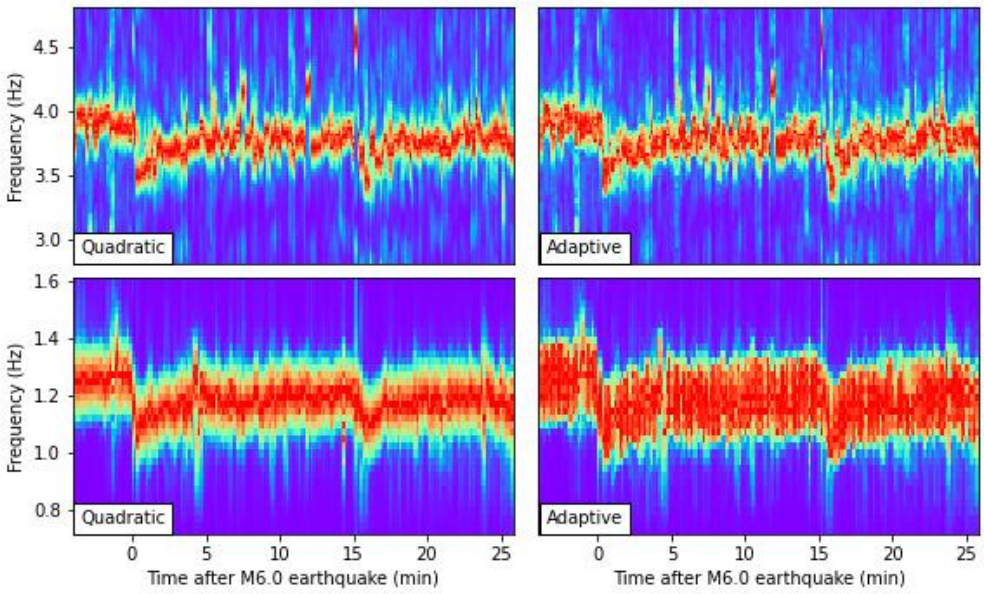

Figure 2: Detailed spectrograms around the vibrational modes of the building show frequency wandering (Clinton et al., 2006) associated with a reduction of the stiffness of the building due to strong shaking. A reduction of the modes is around 10% after the M6.0 earthquakes and slightly less for the M5.8 earthquake. Left and right panels show the spectrogram using the Quadratic and Adaptive multitaper methods, highlighting the improved resolution of the quadratic multitaper, especially around the modal frequency at 1.25 Hz.

The spectral ratio between the mainshock and the EGF spectra is shown in Figure 4. The expected shape of such a spectral ratio has a flat spectrum at lower and higher frequencies and a transition that can be used to find the corner frequencies of the two events (Mayeda et al., 2007; Agurto-Detzel et al., 2017). The spectral ratios shown have the general features expected and it is clear how the spectra of the M6.0 earthquake has a lower corner frequency compared to that of the M5.8 earthquake.

The **`multitaper`** also retains the phase information of the spectral estimates, and thus can estimate the transfer function and by taking its Fourier transform we obtain the source time function (STF) of the mainshock via deconvolution. Figure 4 shows the resulting STF of the M6.0 and M5.8 Mesetas earthquakes using the M4+ earthquakes as EGFs. The resulting STFs confirm what is observed in the spectral ratio, the duration of the M6.0 is greater than that of the M5.8 earthquake. Pseudo-code 3 can be used for obtaining the STF and spectral ratio:\\

Pseudo-Code 3 - Spectral ratio and deconvolution

```
from multitaper import MTSpec, MTCross
Py1   = MTSpec(x1,nw,kspec,dt)
Py2   = MTSpec(x2,nw,kspec,dt)
# Get spectral ratio
sratio = np.sqrt(Py1.spec/Py2.spec)
# Get STF
P12  = MTCross(Py1,Py2,wl=0.001)
xcorr, dcohe, dconv  = P12.mt_corr()
```

where *x1,x2* are the time series of the mainshock and aftershock. Individual spectral estimates are obtained first and later the `mtcross module` is used for calculating the cross-spectrum in variable `P12`, a Python class that holds the cross spectrum of two series. The cross-correlation `xcorr`, normalized cross-correlation `xcohe`, and deconvolution `dcopnv` can be requested (in the time domain). The variable `wl` can be used for stabilizing the deconvolution with a water-level. Figure 4 shows the STF from the `dconv` variable, filtered between 0.2 and 3.0 Hz.

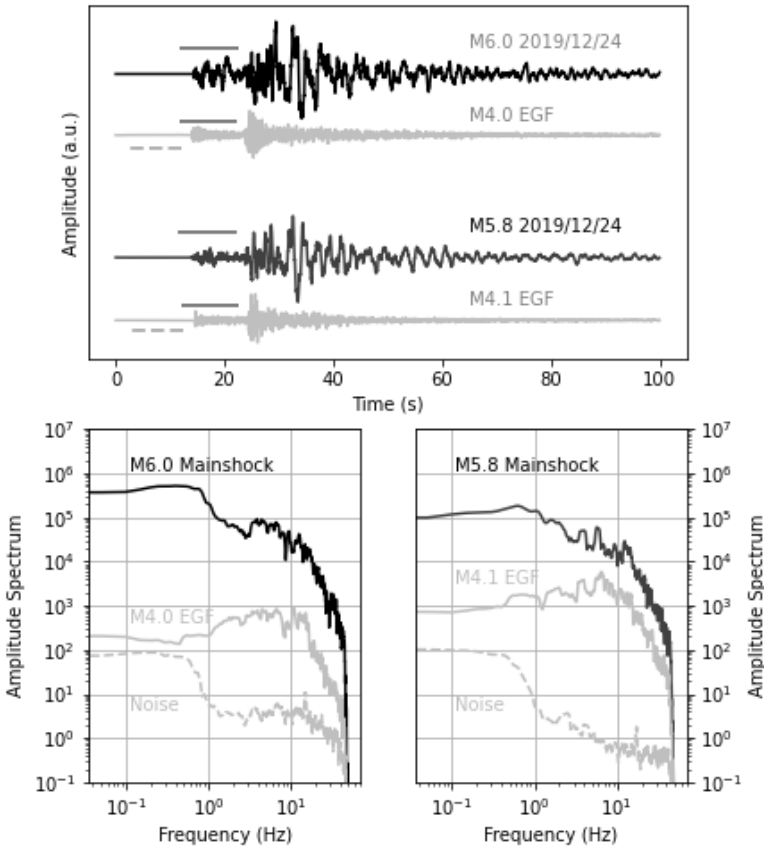

Figure 3: Earthquake source spectrum analysis. Seismograms (top panel) recorded at station PRA (140 km distance) of the M6.0 and M5.8 Mesetas earthquakes and two M4.0 and M4.1 aftershocks that are used as empirical Green's functions (EGF). Corresponding amplitude spectra (bottom panels) using a 10-sec window marked by the horizontal line in each seismogram.

Coherence and correlations between distant frequencies

Waveform similarity can be quantitatively estimated using the coherence. Previous work has shown that even for small aperture arrays waveform similarity decreases quite rapidly from high coherence at low frequencies to low coherence at higher frequencies (Vernon et al., 1991, Qin et al., 2019). Recent studies that use ambient noise have noticed that if the wavefield is fully diffuse, the correlation of different frequencies must be low and that detecting high correlations between distant frequencies can be used as a criterion for diffusive noise (Liu and Ben Zion, 2016, 2018; Liu and Beroza, 2020). Using a similar idea, the coherence between distant frequencies of non-stationary signals – for example dispersive surface waves – is expected to be high (Mellors et al.,

1998; Prieto et al., 2005). The **`multitaper`** allows not only estimating the coherence between two time series, but also the dual-frequency coherence – a matrix of correlations between the spectra at two frequencies (*f1*,*f2*). The dual-frequency coherence can be obtained for a single signal (the signal with itself) or between two signals as shown in Pseudo-Code 4:

Pseudo-Code 4 - Dual-frequency coherence

```
import multitaper.utils as utils
Px   = MTSpec(x,nw,kspec,dt)
Py   = MTSpec(y,nw,kspec,dt)
Sx,Cx,Phx,freq     = utils.df_spec(Px)
Sxy,Cxy,Phxy,freq  = utils.df_spec(Px,Py)
```

where `Cx` is the dual-frequency squared auto-coherence of time series `x`, and `Cxy` is the dual-frequency coherence between `x` and `y` series. The cross-spectrum is stored in `Sxy`, and the phase in `Phxy`.

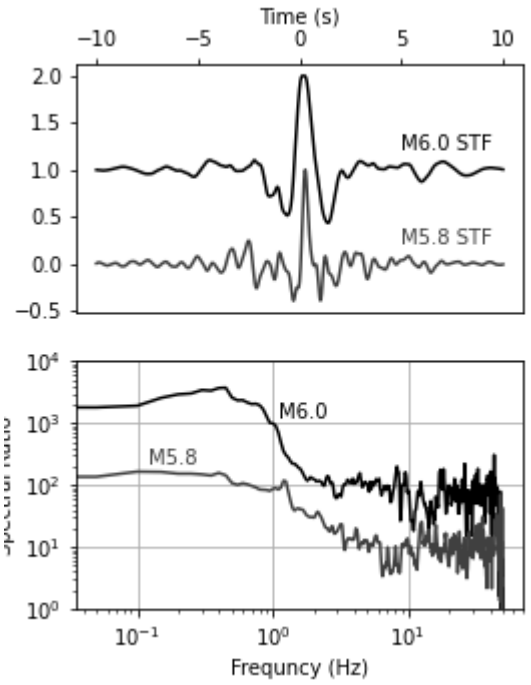

Figure 4: Source time functions (top panel) and spectral ratio (bottom) of the M6.0 and M5.8 using the two M4 earthquakes in Figure 3 as EGFs. Note the shorter STF duration or higher corner frequency of the M5.8 earthquake compared to the M6.0 in this example.

Figure 5 shows two seismic records of the M6.0 and M5.8 Mesetas earthquakes recorded at two nearby stations (VMM07 and VMM11) in a deep sedimentary basin. The two stations are separated 32 km and are about 520 km from the epicenter. For this example, I select 3 windows, a noise window (noise), a window with the surface wave of the M6.0 earthquake (mainshock), and the full trace of the M5.8 earthquake (aftershock). For each window, we calculate the dual-frequency coherence for a single station and between the two stations.

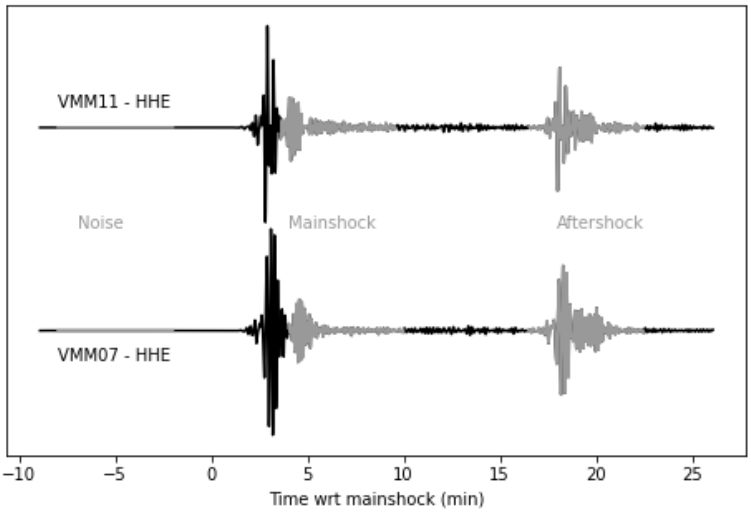

Figure 5: Recorded seismograms at two nearby stations (station separation 32 km, source-receiver separation 520 km). Three windows are selected for studying the correlation between neighboring frequencies using dual-frequency coherence estimates. The three windows include a noise window (noise), the surface wave of the M6.0 earthquake (mainshock), and the full trace of the M5.8 earthquake (aftershock).

Figure 6 shows the resulting dual-frequency coherence for the windows selected. The auto-coherence of the noise window for station VMM07 shows low values for off-diagonal terms, while the mainshock and aftershock windows show significant coherence in the off-diagonal terms. For the mainshock window the off-diagonal terms have high amplitudes between about 0.9 and 0.16 Hz, suggesting a non-diffuse dispersive wave – note the main diagonal is always 1 for auto-coherence.

The dual-frequency coherence between the two stations for the noise window shows low coherence over all frequencies, confirming the diffusive nature of the wavefield. In contrast, the mainshock window shows significant coherence in the off-diagonal terms. The coherence along the main diagonal has high coherence between 0.09 and 0.12 Hz but drops rapidly at higher frequencies, while the off-diagonal terms have high coherence up to 0.16 Hz. The off-diagonal coherence is asymmetric with respect to the diagonal and has a different slope suggesting that the nature of the dispersion curve of the surface waves at the two stations is different.

Conclusions

This work presents a Python package for multitaper spectral analysis. A number of examples display the different capabilities of `multitaper` for estimating the power spectral density, spectral ratio and deconvolutions or dual-frequency coherencies. Other functions that include F-test for periodic components or application of the sine multitaper are also available and are documented in the GitHub repository. The multitaper algorithm has been widely used in geophysics, economics, medicine, climate and of course seismology and this contribution aims at expanding the available tools for studying the Earth.

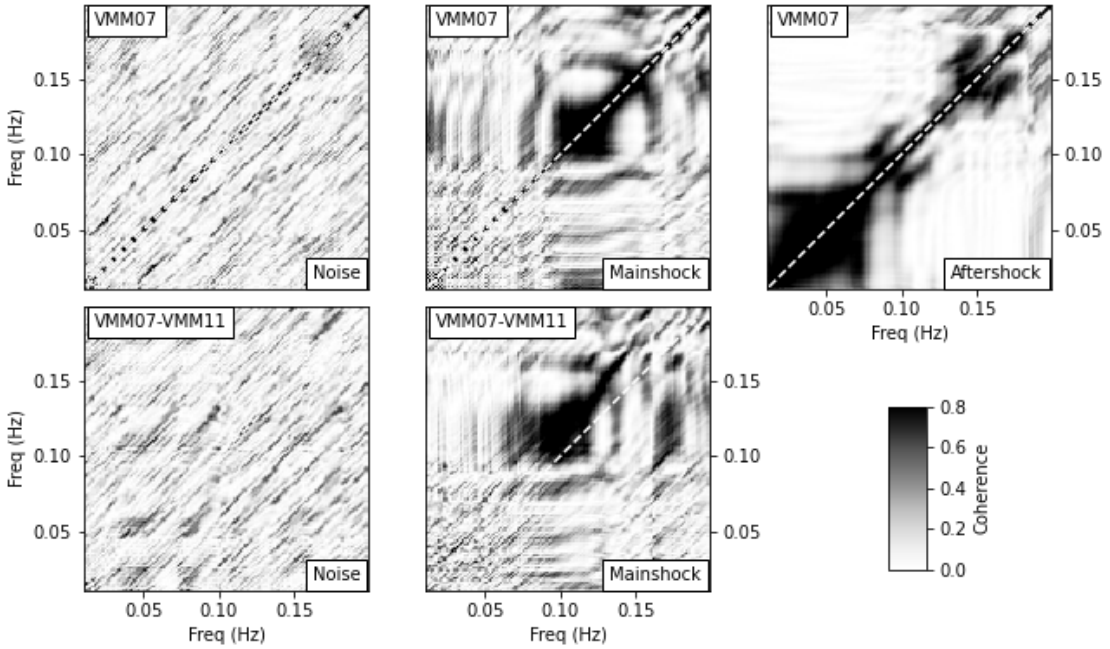

Figure 6: Coherence between neighboring frequencies. The dual-frequency auto-coherence estimated from the noise, mainshock and aftershock windows for station VMM07 (upper row) and the coherence between stations VMM07 and VMM11 for the noise and mainshock windows. Note how the coherence is low in the off-diagonal for the noise windows (diffusive noise) while for the two other windows a higher coherence is observed in the off-diagonal. The interstation coherence for the mainshock window (surface wave) has a high correlation away from the main diagonal between 0.10-0.15 Hz, which can be interpreted as surface waves with distinct dispersion characteristics.

Data and Resources

The `multitaper` package, scripts, and Jupyter Notebooks to reproduce the figures in this contribution are available on GitHub (https://github.com/gaprieto/multitaper). The data used here as examples comes from the Servicio Geológico Colombiano (SGC) and from a temporary deployment in the Crisanto building (Bogota) as part of a project supported by ECCI University. The SGC data are available at http://sismo.sgc.gov.co:8080 (last accessed January 2021) and were downloaded using Obspy (Beyreuther et al., 2010) and the Client.get_waveforms function. The seismic and building data used in the examples is available in a Zenodo repository (10.5281/zenodo.6025794).

Acknowledgments

Special thanks to SGC and ECCI University for making the data available. I would like to thank the Pascal Audet and one anonymous reviewer that helped significantly improve user's experience for downloading, installing and documentation access.

References

Abercrombie, R. E. (2015). Investigating uncertainties in empirical Green's function analysis of earthquake source parameters. *Journal of Geophysical Research: Solid Earth*, *120*(6), 4263-4277.

Agurto-Detzel, H., Bianchi, M., Prieto, G. A., & Assumpção, M. (2017). Earthquake source properties of a shallow induced seismic sequence in SE Brazil. *Journal of Geophysical Research: Solid Earth*, *122*(4), 2784-2797.

Båth, B. M. (1974). *Spectral analysis in geophysics*. Elsevier.

Beyreuther, M., Barsch, R., Krischer, L., Megies, T., Behr, Y., & Wassermann, J. (2010). ObsPy: A Python toolbox for seismology. *Seismological Research Letters*, *81*(3), 530-533.

Bonilla, L. F., Guéguen, P., & Ben-Zion, Y. (2019). Monitoring coseismic temporal changes of shallow material during strong ground motion with interferometry and autocorrelation. *Bulletin of the Seismological Society of America*, *109*(1), 187-198.

Bracewell, R. N. (2000). The Fourier transform and its applications. 3rd Edition. pp. 616. New York: McGraw-Hill.

Chaves, E. J., Schwartz, S. Y., & Abercrombie, R. E. (2020). Repeating earthquakes record fault weakening and healing in areas of megathrust postseismic slip. *Science advances*, *6*(32), eaaz9317.

Clinton, J. F., Bradford, S. C., Heaton, T. H., & Favela, J. (2006). The observed wander of the natural frequencies in a structure. *Bulletin of the seismological society of America*, *96*(1), 237-257.

Cossette, É., Audet, P., Schneider, D., & Grasemann, B. (2016). Structure and anisotropy of the crust in the Cyclades, Greece, using receiver functions constrained by in situ rock textural data. *Journal of Geophysical Research: Solid Earth*, *121*(4), 2661-2678.

Dannemann Dugick, F. K., van der Lee, S., Prieto, G. A., Dybing, S. N., Toney, L., & Cole, H. M. (2021). ROSES: Remote Online Sessions for Emerging Seismologists. *Seismological Research Letters*, *92*(4), 2657-2667.

Diagourtas, D., Tzanis, A., & Makropoulos, K. (2002). Comparative study of microtremor analysis methods. In *Earthquake Microzoning* (pp. 2463-2479). Birkhäuser, Basel.

Gibbons, S. J., Harris, D. B., Dahl-Jensen, T., Kværna, T., Larsen, T. B., Paulsen, B., & Voss, P. H. (2017). Locating seismicity on the Arctic plate boundary using multiple-event techniques and empirical signal processing. *Geophysical Journal International*, *211*(3), 1613-1627

Haley, C. L., & Geoga, C. J. (2020). Multitaper. jl: A Julia package for frequency domain analysis of time series. *Journal of Open Source Software*, *5*(55), 2463

Häusler, M., Michel, C., Burjánek, J., & Fäh, D. (2021). Monitoring the Preonzo rock slope instability using resonance mode analysis. *Journal of Geophysical Research: Earth Surface*, *126*(4), e2020JF005709.

Hough, S. E. (1997). Empirical Green's function analysis: Taking the next step. *Journal of Geophysical Research: Solid Earth*, *102*(B3), 5369-5384.

Jang, H., Kim, Y., Lim, H., & Clayton, R. W. (2019). Seismic attenuation structure of southern Peruvian subduction system. *Tectonophysics*, *771*, 228203

Jaimes, N., Prieto, G.A., Rodriguez, C. (2022). Detection of Building Response Changes Using Deconvolution Interferometry: A Case Study in Bogota, Colombia. Seism. Res. Lett. 93(2A). 931-942. doi: 10.1785/0220210219

Kay, S. M., & Marple, S. L. (1981). Spectrum analysis—A modern perspective. *Proceedings of the IEEE*, *69*(11), 1380-1419.

Kemna, K. B., Peña Castro, A. F., Harrington, R. M., & Cochran, E. S. (2020). Using a large-n seismic array to explore the robustness of spectral estimations. *Geophysical Research Letters*, *47*(21), e2020GL089342

Kong, Q., Allen, R. M., Kohler, M. D., Heaton, T. H., & Bunn, J. (2018). Structural health monitoring of buildings using smartphone sensors. *Seismological Research Letters*, *89*(2A), 594-602.

Larsen Y. and A. Hanssen (2004). "Dual-frequency dual-wavenumber cross-coherence of nonstationary and inhomogeneous harmonizable random fields," in Proc. IEEE Int. Conf. Acoust., Speech, Signal Process, Montreal, QC, Canada, pp. II–625–II–628, IEEE.

Lees, J. M., & Park, J. (1995). Multiple-taper spectral analysis: A stand-alone C-subroutine. *Computers & Geosciences*, *21*(2), 199-236.

Liu, X., & Ben-Zion, Y. (2016). Estimating correlations of neighboring frequencies in ambient seismic noise. *Geophysical Journal International*, *206*(2), 1065-1075.

Liu, X., & Ben-Zion, Y. (2018). Analysis of non-diffuse characteristics of the seismic noise field in southern California based on correlations of neighboring frequencies. *Geophysical Journal International*, *212*(2), 798-806.

Liu, X., & Beroza, G. C. (2020). Quantifying the effects of nondiffuse noise on ballistic and coda wave amplitude from variances of seismic noise interferometry in Southern California. *Journal of Geophysical Research: Solid Earth*, *125*(1), e2019JB017617.

Liu, Z., Park, J., & Karato, S. I. (2018). Seismic evidence for water transport out of the mantle transition zone beneath the European Alps. *Earth and Planetary Science Letters*, *482*, 93-104.

Madariaga, R., Ruiz, S., Rivera, E., Leyton, F., & Baez, J. C. (2019). Near-field spectra of large earthquakes. *Pure and Applied Geophysics*, *176*(3), 983-1001.

Mayeda, K., Malagnini, L., & Walter, W. R. (2007). A new spectral ratio method using narrow band coda envelopes: Evidence for non-self-similarity in the Hector Mine sequence. *Geophysical Research Letters*, *34*(11).

Mayorga, E., Dionicio, V., Lizarazo, M., Pedraza, P., Poveda, E., Mercado, O., Siervo, D., Aguirre, L., Bolaños, R., Garzón, F., Velásquez, L., Castillo, L., García, H., Mazo, E., Arcila, M., Barbosa, D., Sarabia, A., López, M., Días, F., Valcárcel, J., … Bohórquez, O. (2020). EL SISMO DE MESETAS, META DEL 24 DE DICIEMBRE DE 2019 Aspectos sismológicos, movimiento fuerte y consideraciones geodésicas. Bogotá: Servicio Geológico Colombiano (link).

Melgar, D., Crowell, B. W., Melbourne, T. I., Szeliga, W., Santillan, M., & Scrivner, C. (2020a). Noise characteristics of operational real-time high-rate GNSS positions in a large aperture network. *Journal of Geophysical Research: Solid Earth*, *125*(7), e2019JB019197.

Melgar, D., Melbourne, T. I., Crowell, B. W., Geng, J., Szeliga, W., Scrivner, C., ... & Goldberg, D. E. (2020b). Real-time high-rate GNSS displacements: Performance demonstration during the 2019 Ridgecrest, California, earthquakes. *Seismological Research Letters*, *91*(4), 1943-1951.

Mellors, R. J., Vernon, F. L., & Thomson, D. J. (1998). Detection of dispersive signals using multitaper dual-frequency coherence. *Geophysical Journal International*, *135*(1), 146-154.

Morelli, A., Zaccarelli, L., Cavaliere, A., & Azzara, R. M. (2021). Normal Modes of a Medieval Tower Excited by Ambient Vibrations in an Urban Environment. *Seismological Research Letters*.

Mueller, C. S. (1985). Source pulse enhancement by deconvolution of an empirical Green's function. *Geophysical Research Letters*, *12*(1), 33-36.

Noriega-Londoño, S., Bermúdez, M.A., Restrepo-Moreno, S.A., Marín-Cerón, M.I., García-Delgado, H., 2021, Earthquake ground deformation using DInSAR analysis and instrumental seismicity: The 2019 M 6.0 Mesetas Earthquake, Meta, Colombian Andes: Boletín de la Sociedad Geológica Mexicana, 73 (2), A090221. http://dx.doi.org/10.18268/BSGM2021v73n2a090221

Olafsson, S., & Sigbjörnsson, R. (1995). Application of ARMA models to estimate earthquake ground motion and structural response. *Earthquake engineering & structural dynamics*, *24*(7), 951-966.

Pardo-Igúzquiza, E., Chica-Olmo, M., & Rodríguez-Tovar, F. J. (1994). CYSTRATI: a computer program for spectral analysis of stratigraphic successions. *Computers & Geosciences*, *20*(4), 511-584

Percival, D. B., & Walden, A. T. (1993). *Spectral analysis for physical applications*. Cambridge University Press.

Prieto, G. A., Vernon, F. L., Masters, G., & Thomson, D. J. (2005). Multitaper Wigner-Ville spectrum for detecting dispersive signals from earthquake records. In Conference Record of the Thirty-Ninth Asilomar Conference on Signals, Systems and Computers, 2005. pp. 938-941. IEEE.

Prieto, G. A., Parker, R. L., Thomson, D. J., Vernon, F. L., & Graham, R. L. (2007). Reducing the bias of multitaper spectrum estimates. *Geophysical Journal International*, *171*(3), 1269-1281.

Prieto, G., Parker , R., & Vernon III, F. (2009). A Fortran 90 library for multitaper spectrum analysis. *Computers & Geosciences, Vol. 35, pp. 1701–1710*.

Qin, L., Vernon, F. L., Johnson, C. W., & Ben-Zion, Y. (2019). Spectral characteristics of daily to seasonal ground motion at the Piñon Flats Observatory from coherence of seismic data. *Bulletin of the Seismological Society of America*, *109*(5), 1948-1967.

Rahim KJ, Burr WS, Thomson DJ (2014). *Applications of Multitaper Spectral Analysis to Nonstationary Data*. Ph.D. thesis, Queen's University. R package version 1.0-15, https://CRAN.R-project.org/package=multitaper

Thomson, D. J. (1982). Spectrum estimation and harmonic analysis. *Proceedings of the IEEE*, *70*(9), 1055-1096.

Thomson, D.J. and F. L. Vernon (1998). "Signal extraction via multitaper spectra of non-stationary data," in Proceedings of the Thirty-Second Asilomar Conf. on Signals, Systems and Computers, Madison, WI., IEEE, pp. 271–275, Omnipress.

Trugman and Savvaidis, A. (2021). Source Spectral Properties of Earthquakes in the Delaware Basin of West Texas. *Seismological Research Letters*.

Tary, J. B., Herrera, R. H., Han, J., & van der Baan, M. (2014). Spectral estimation—What is new? What is next?. *Reviews of Geophysics*, *52*(4), 723-749.

Ugalde, A., Egozcue, J. J., & Ranero, C. R. (2021). A new autoregressive moving average modeling of H/V spectral ratios to estimate the ground resonance frequency. *Engineering Geology*, *280*, 105957.

Vernon, F. L., Fletcher, J., Carroll, L., Chave, A., & Sembera, E. (1991). Coherence of seismic body waves from local events as measured by a small-aperture array. *Journal of Geophysical Research: Solid Earth*, *96*(B7), 11981-11996.